nature nanotechnology

Article

https://doi.org/10.1038/s41565-022-01272-4

Hydrogen-substituted graphdiyne-assisted ultrafast sparking synthesis of metastable nanomaterials

Received: 31 January 2022

Accepted: 20 October 2022

Published online: 30 December 2022

Check for updates

Xueli Zheng[1,5], Xin Gao[1,5], Rafael A. Vilá[1], Yue Jiang[2], Jingyang Wang[1], Rong Xu[1], Rui Zhang[3], Xin Xiao[1], Pu Zhang[1], Louisa C. Greenburg[1], Yufei Yang[1], Huolin L. Xin[3], Xiaolin Zheng[2] & Yi Cui[1,4]

Metastable nanomaterials, such as single-atom and high-entropy systems, with exciting physical and chemical properties are increasingly important for next-generation technologies. Here, we developed a hydrogen-substituted graphdiyne-assisted ultrafast sparking synthesis (GAUSS) platform for the preparation of metastable nanomaterials. The GAUSS platform can reach an ultra-high reaction temperature of 3,286 K within 8 ms, a rate exceeding 10^5 K s^{-1}. Controlling the composition and chemistry of the hydrogen-substituted graphdiyne aerogel framework, the reaction temperature can be tuned from 1,640 K to 3,286 K. We demonstrate the versatility of the GAUSS platform with the successful synthesis of single atoms, high-entropy alloys and high-entropy oxides. Electrochemical measurements and density functional theory show that single atoms synthesized by GAUSS enhance the lithium–sulfur redox reaction kinetics in all-solid-state lithium–sulfur batteries. Our design of the GAUSS platform offers a powerful way to synthesize a variety of metastable nanomaterials.

Metastable nanomaterials are a class of materials with unique physical and chemical properties that are different from their equilibrium and bulk phases[1,2]. These properties offer the opportunity to develop next-generation technologies, including renewable energy[3,4], electric vehicles[5–7] and materials manufacturing[2,8,9]. For instance, single-atom metastable materials with abundant unsaturated active sites and strong metal–support interaction enable electrocatalysis and thermal catalysis for chemical upgrade[10,11]. Metastable high-entropy alloys represent an ideal prototype for investigating the electrocatalytic and mechanical processes, from fundamentals to applications[8,12]. However, these metastable nanomaterials are very challenging to synthesize due to their requirement for extreme non-equilibrium synthesis conditions.

High-temperature strategies using conventional resistive-heating furnaces have attracted extensive attention for synthesizing metastable nanomaterials, but are usually limited to single-component metastable materials[6,13,14]. High-entropy materials with five or more elements are challenging to achieve owing to the limited temperatures (~1,500 K) and heating rates (only 10–20 K min^{-1}) of furnace annealing. Recently, advanced high-temperature synthesis has opened an avenue to create non-equilibrium conditions and avoid phase segregation for synthesizing a variety of metastable nanomaterials[3,15]. For example, laser ablation in liquids with rapid quenching rates was developed to synthesize metastable single-atom alloys[16]. High-temperature shock synthesis with a superfast heating speed was utilized to design high-entropy alloys and oxides[3,4,17]. An aerosol droplet-mediated approach with a temperature higher than 2,000 K was developed to synthesize high-entropy alloys[18,19]. However, ultra-high temperatures (>3,000 K) and ultrafast heating rates (>10^5 K s^{-1}) are still challenging to achieve, but are increasingly important for materials synthesis and manufacture[20–23]. Facile synthesis achieving ultra-high temperatures

[1]Department of Materials Science and Engineering, Stanford University, Stanford, CA, USA. [2]Department of Mechanical Engineering, Stanford University, Stanford, CA, USA. [3]Department of Physics and Astronomy, University of California, Irvine, CA, USA. [4]Stanford Institute for Materials and Energy Sciences, SLAC National Accelerator Laboratory, Menlo Park, CA, USA. [5]These authors contributed equally: Xueli Zheng, Xin Gao. e-mail: yicui@stanford.edu

https://doi.org/10.1038/s41565-022-01272-4

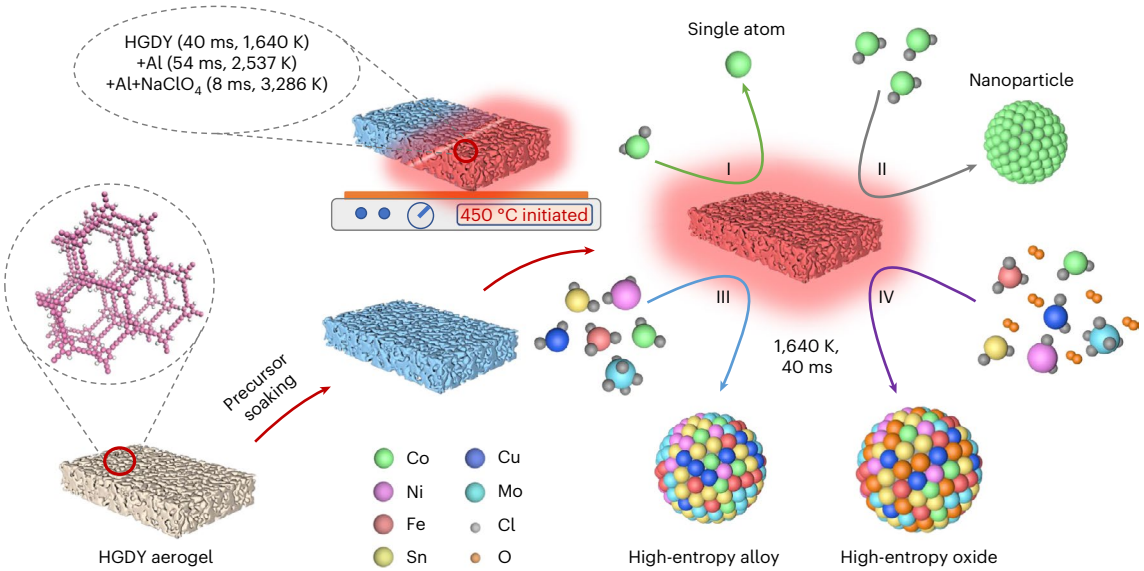

Fig. 1 | Schematic of hydrogen-substituted GAUSS for metastable nanomaterials. Precursors are first dissolved in ethanol and soaked on HGDY aerogel. Solvated HGDY aerogel is dried and placed on the hotplate set at a temperature of 450 °C. Immediately, a sparking reaction occurs and spreads quickly through the entire aerogel, achieving an ultra-high temperature up to 3,286 K within 8 ms. By establishing the GAUSS platform, we successfully synthesize a group of metastable nanomaterials, including single atoms using dilute single-metal precursors, nanoparticles using a concentrated single-metal precursor and high-entropy alloys and oxides using multi-metal precursors. The green, purple, red, yellow, dark blue, light blue, grey and orange atoms represent Co, Ni, Fe, Sn, Cu, Mo, Cl and O, respectively.

within milliseconds is strongly desired for developing a library of metastable nanomaterials.

In this work, we developed an ultrafast high-temperature platform with the help of hydrogen-substituted graphdiyne aerogel (HGDY). HGDY, a two-dimensional sp/sp^2 co-hybridized carbon network, provides high density sites for supporting metastable nanomaterials[24–26]. Our designed hydrogen-substituted graphdiyne-assisted ultrafast sparking synthesis (GAUSS) achieves a temperature of 1,640 K within 40 ms. By incorporating aluminium nanoparticles and oxidizers, GAUSS reaches a remarkable temperature of 3,286 K within only 8 ms, a heating rate greater than 10^5 K s^{-1}. We successfully synthesized a library of metastable nanomaterials, including single atoms, high-entropy alloys and high-entropy oxides using the GAUSS platform. Finally, electrochemical measurements and density functional theory show that single-atom catalysts synthesized with the GAUSS platform promote lithium–sulfur (Li–S) conversion kinetics in all-solid-state Li–S batteries.

Results and discussion

Graphdiyne-assisted ultrafast sparking synthesis

For the GAUSS process, the HGDY aerogel is designed to provide micro-explosions. HGDY aerogels have high surface area, high volume to mass ratio, micropores and unique acetylenic carbon chemistry (Supplementary Fig. 1), which provide high density sites of micro-explosions to realize ultra-high temperature. When the HGDY aerogel touches the hotplate (set to 450 °C) a sparking reaction occurs. During this reaction, red flames spread quickly from their origin through the entire aerogel, transforming the HGDY from a light brown to black colour (Supplementary Fig. 2). This reaction produces a large amount of heat and pressure. The temperature of the reaction can be controlled from 1,600 K up to 3,286 K, while the reaction time can also be controlled from 40 ms to 8 ms by tuning the chemistry of the aerogel (Fig. 1).

Using the high reaction temperature and fast heating rates of our GAUSS platform, we synthesize a variety of metastable nanomaterials, including single atoms (with dilute single-metal precursors), metal nanoparticles (with concentrated single-metal precursors), high-entropy alloys (with multi-metal precursors in an argon atmosphere) and high-entropy oxides (with multi-metal precursors in an oxygen-rich atmosphere) (Fig. 1). As a proof of concept, we showcase the synthesis of cobalt (Co) single atoms, Co nanoparticles, NiFeCoCuSnMo alloys and NiFeCoCuSnMo oxides. Synthesis of these metastable nanomaterials with our GAUSS platform is achieved by soaking the HGDY aerogel in ethanol with dissolved metal salts and then drying, to achieve a metal-infused HGDY aerogel. The metal-infused HGDY aerogel is then placed in contact with a hotplate (set to 450 °C), quickly initiating the spark reaction, which provides the fast heating and cooling rates necessary to achieve the metastable states. The facile, scalable nature and low costs of reagents for the GAUSS platform endow the method with promise for large-scale commercialization (Supplementary Table 1). The GAUSS platform involves the following processes: sol-gel method to prepare the carbon aerogel, solution method to soak metal precursors, drying the solvated carbon aerogels and using the hotplate to provide heat for initializing the GAUSS reaction. Each process is scalable and low cost.

To analyse the temperature and heating rates of the GAUSS synthesis, we use a high-speed camera (Fig. 2a–d) and a thermal camera (Fig. 2e–h). Note that different samples were used for the high-speed camera and thermal camera observations. Snapshots of the sparking reaction show that ignition occurs at a single point (Fig. 2a,e), spreads through the entire HGDY aerogel within 19 ms (Fig. 2b,f) and achieves a maximum temperature of 1,600 K at 40 ms (Fig. 2c,g). Plotting temperature versus time with millisecond intervals (Fig. 2i), we found a very high heating rate exceeding 10^5 K s^{-1}. To validate the measured heating rates and temperatures of the spark reaction, we constructed a COMSOL model to simulate the temperature profile during the reaction. The temperature trend from COMSOL agrees well with the measured temperature profile (Fig. 2i).

To understand the chemical changes of HGDY during the spark reaction, we performed C 1*s* X-ray photoelectron spectroscopy (XPS) before and after the GAUSS process. High-resolution C 1*s* spectra show that the ratio of C=C bonds to C≡C bonds increases after the GAUSS process, indicating cleavage of terminal acetylenic bonds (Supplementary

https://doi.org/10.1038/s41565-022-01272-4

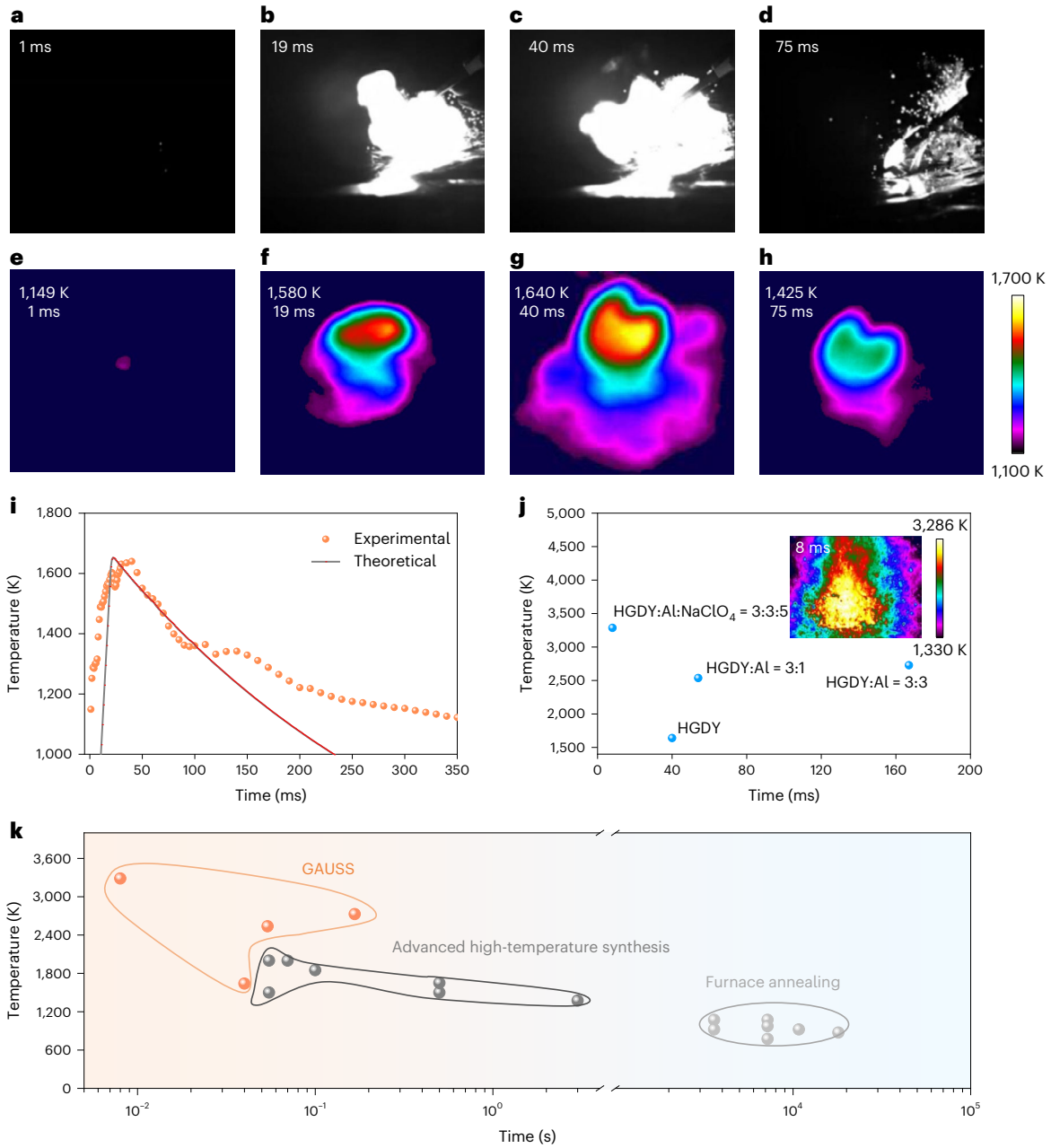

Fig. 2 | Temperature evolution and mechanism of the GAUSS process. **a**–**h**, High-speed camera video snapshots at 1 ms (**a**), 19 ms (**b**), 40 ms (**c**) and 75 ms (**d**), and the corresponding thermal camera video snapshots showing temperatures of 1,149 K (**e**), 1,580 K (**f**), 1,640 K (**g**) and 1,425 K (**h**) during the GAUSS process. **i**, Experimental (scattered) and simulated (solid) temperature profile of GAUSS. **j**, The highest temperature during the GAUSS process after incorporating corresponding amounts of aluminium (Al) nanoparticles and sodium perchlorate ($NaClO_4$) oxidizers. Inset shows the highest temperature of 3,286 K at 8 ms with a HGDY:Al:$NaClO_4$ mass ratio of 3:3:5. **k**, Time and temperature comparison of the developed GAUSS with advanced high-temperature synthesis[3,4,18–20,27,31] and furnace annealing[5,6,13,14,32–34]. The exact temperature and time for different conditions are summarized in Supplementary Table 2.

Fig. 3), formation of C=C bonds and release of heat. The evolution of hydrogen and hydrocarbons during the GAUSS process further confirms the cleavage of terminal C≡C bonds (Supplementary Fig. 4).

To accelerate the heating and increase the ultimate temperature of the GAUSS process, we incorporated aluminium nanoparticles and sodium perchlorate ($NaClO_4$) oxidizers into the HGDY aerogel (Fig. 2j and Supplementary Figs. 5–7). Aluminium nanoparticles with high specific energy density (31 kJ g^{-1}) are used as the fuel to increase the temperature of GAUSS. $NaClO_4$ is a stronger oxidizer and decomposes into oxygen to increase the ramping rate of GAUSS. The fastest heating rate and highest temperature were achieved using a 3:3:5 mass ratio of HGDY:Al:$NaClO_4$. We measured a maximum temperature of 3,286 K within 8 ms, with a heating rate of ~4×10^5 K s^{-1} (Supplementary Fig. 7 and inset of Fig. 2j). Our approach to add aluminium nanoparticles and sodium perchlorate oxidizers, that is, soak the precursors onto the HGDY support, is easy, scalable and low cost. Adding aluminium also provides potential opportunities to study the metal–support interaction and thermal catalysis. We compare our GAUSS platform with reported synthesis methods for metastable nanomaterials, showing the exciting combination of very high temperature and heating rates in our GAUSS platform (Fig. 2k). Conventional annealing furnaces usually need ~1,100 K and several hours for metastable nanomaterial

https://doi.org/10.1038/s41565-022-01272-4

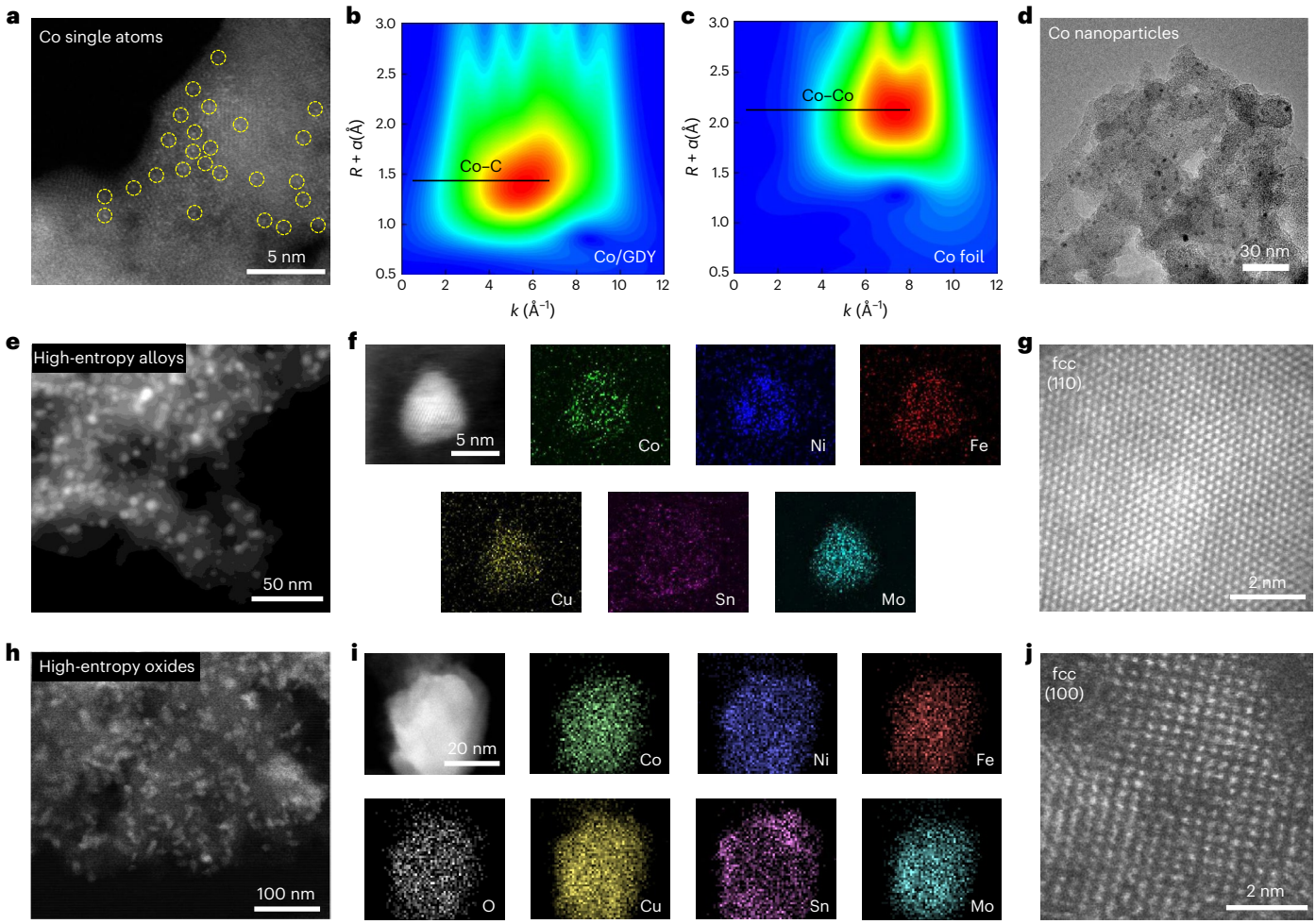

Fig. 3 | Characterization of a series of metastable nanomaterials, including single atoms, high-entropy alloy and high-entropy oxide, by GAUSS. a, STEM image of Co single atoms on HGDY. **b**,**c**, Wavelet transforms for Co-HGDY (**b**) and Co foil reference (**c**). **d**, TEM image of Co nanoparticles on HGDY. **e**,**f**, STEM image (**e**) and EDS (**f**) mappings of as-prepared high-entropy alloys containing six elements (Co, Ni, Fe, Cu, Sn and Mo) on HGDY by GAUSS. **g**, Atomic-scale HAADF-STEM image of high-entropy alloys; fcc, face-centred cubic. **h**,**i**, STEM image (**h**) and EDS mappings (**i**) of as-prepared high-entropy oxide nanoparticles on HGDY by GAUSS. **j**, Atomic-scale HAADF-STEM image of high-entropy oxides.

synthesis. Recent advanced high-temperature synthesis reported by Hu and co-authors reached around 2,000 K within 55 ms (refs. 3,27). Our work represents a step forward by achieving a temperature higher than 3,286 K in 8 ms (Supplementary Table 2). The high temperature and fast time are very important to access highly non-equilibrium states of materials. Moreover, the ultrafast heating speed gives a much higher energy efficiency than conventional heating approaches.

Metastable nanomaterials achieved using GAUSS

With the GAUSS platform, we demonstrate that a variety of metastable nanomaterials can be synthesized by tuning the reaction precursors and sparking atmosphere. Here we synthesized single atoms, high-entropy alloy nanoparticles and high-entropy oxide nanoparticles. To characterize single atoms produced by our GAUSS platform, we use aberration-corrected high-angle annular dark-field scanning transmission electron microscopy (HAADF-STEM) to resolve single atoms owing to the large atomic number difference between metal atoms and carbon atoms in the HGDY support. The HAADF-STEM image shows localized bright spots on the HGDY support, indicating that single-atom Co sites are well dispersed on the HGDY support (Fig. 3a). Co K-edge extended X-ray absorption fine structure further supports the HAADF-STEM measurements. Wavelet analysis shows no Co–Co formation in the Co/HGDY material, indicating the successful synthesis of single-atom sites on HGDY (Fig. 3b,c). On the basis of density functional theory (DFT) simulation, we believe the likely adsorption sites for Co single atoms are at butadiyne linkages (–C≡C–C≡C–, *sp*-hybridized carbon) given the favourable adsorption geometry (Supplementary Fig. 8). The Co loading is determined as 0.23 wt% by inductively coupled plasma analysis. Increasing the concentration of $CoCl_2{\cdot}6H_2O$ precursor to 5 mM, we find that Co nanoparticles with a size distribution of 2.7 nm are synthesized, showing that precursor concentration and dispersion are important to achieve single atoms with our GAUSS platform (Fig. 3d and Supplementary Fig. 9).

High-entropy alloy nanoparticles can be synthesized with the GAUSS process by mixing multi-metal salt precursors and soaking the HGDY aerogel in homogeneous multi-metal precursors. Here, we chose six metal chloride precursors (Fe, Co, Ni, Cu, Sn and Mo) to synthesize high-entropy alloy nanoparticles. An average particle size of 5 nm is uniformly distributed on the HGDY support (Fig. 3e). STEM-energy dispersive spectroscopy (EDS) mapping shows the uniform distribution of multi-metal in the high-entropy alloy particle (Fig. 3f). Controlling the atmosphere of the GAUSS platform enables the reaction between gas molecules and the high-entropy metal. Here, we perform the GAUSS reaction of the high-entropy NiFeCoCuSnMo system in an oxygen-rich atmosphere to synthesize high-entropy oxide (NiFeCoCuSnMoO) nanoparticles on HGDY. The HAADF-STEM image of the synthesized

https://doi.org/10.1038/s41565-022-01272-4

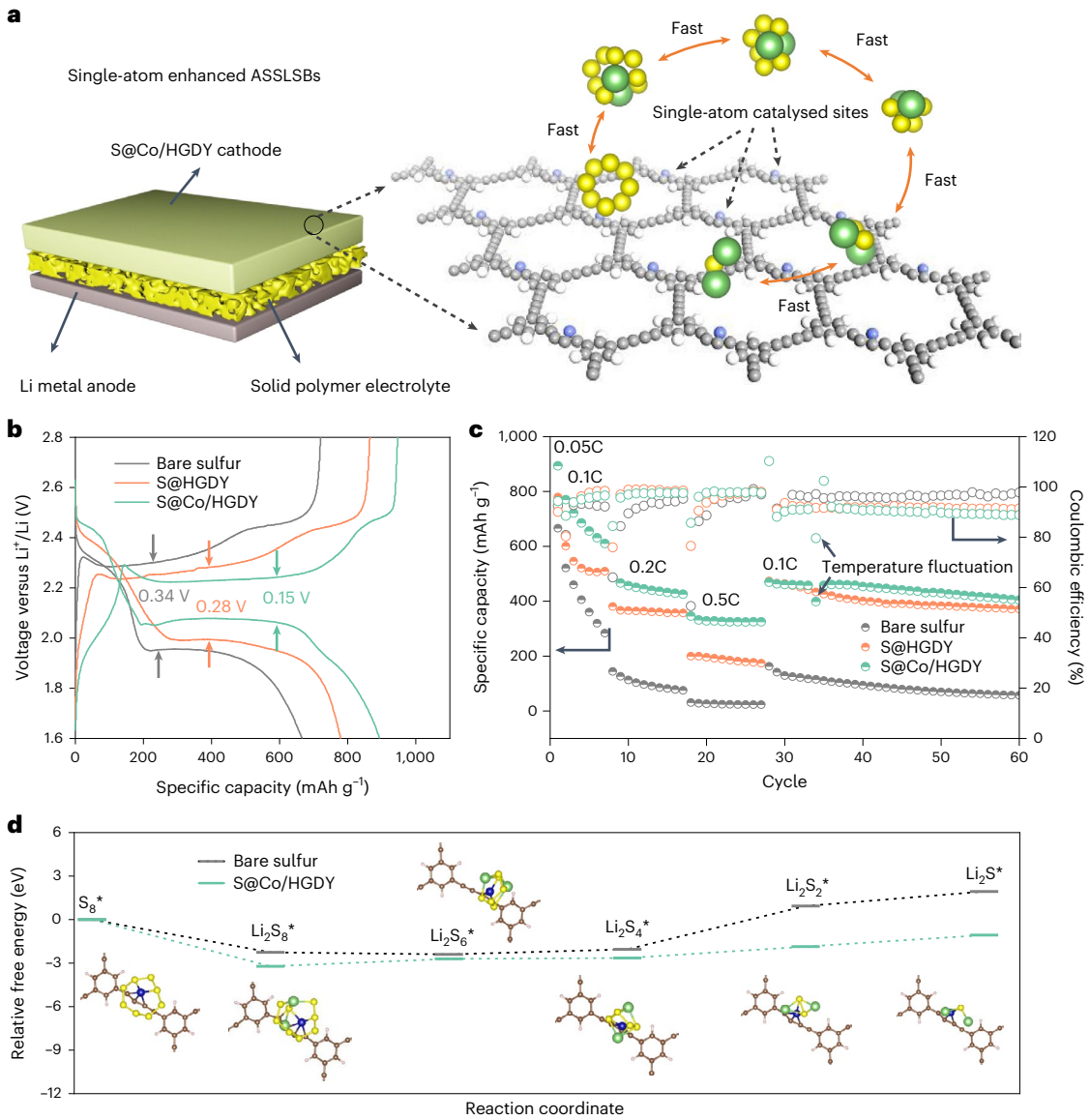

Fig. 4 | Ultrafast single-atom synthesis for ASSLSBs. a, Schematic of Co single-atom-enabled ultrafast Li–S conversion in ASSLSBs. **b**, Charge–discharge curves of ASSLSBs using bare sulfur cathodes, S@HGDY cathodes and S@Co/HGDY cathodes at 60 °C and 0.05C. **c**, Rate and cycling performance of ASSLSBs using bare sulfur cathodes, S@HGDY cathodes and S@Co/HGDY cathodes at 60 °C. **d**, Energy profiles for the reduction of bare sulfur and sulfur@Co/HGDY. The optimized structures of the intermediates are shown in the inset.

high-entropy oxide nanoparticles in Fig. 3h shows the uniform distribution on the HGDY support. The average particle size of high-entropy oxides is four times larger than that of the high-entropy alloys, owing to addition of oxygen atoms into particles during the reaction in the oxygen-rich atmosphere. The elemental distribution of oxygen and metals in the high-entropy oxides was verified by EDS mapping (Fig. 3i). Atomic-scale HAADF-STEM images of high-entropy alloy nanoparticles and high-entropy oxide nanoparticles show a face-centred cubic crystalline structure (Fig. 3g,j). The atomic ratio of high-entropy alloy nanoparticles and high-entropy oxide nanoparticles is measured as $Ni_{0.27}Fe_{0.15}Co_{0.19}Cu_{0.38}Sn_{0.11}Mo_{0.24}$ and $Ni_{0.25}Fe_{0.27}Co_{0.23}Cu_{0.52}Sn_{0.09}Mo_{0.33}O$ (Supplementary Table 3). The C 1*s* XPS for high-entropy alloy nanoparticles and high-entropy oxide nanoparticles on HGDY indicates that HGDY is oxidized if GAUSS is performed in an oxygen-rich atmosphere (Supplementary Fig. 10).

To demonstrate the generalization of the GAUSS platform, we extended the approach using graphene oxide as the starting material. STEM images and EDS elemental mapping show that high-entropy alloy NiFeCoCuSnMo was successfully synthesized on reduced graphene oxide using GAUSS (Supplementary Figs. 11 and 12). Snapshots of the thermal camera video show that the highest temperature reached was 1,265 K within 11 ms (Supplementary Fig. 13).

Single atoms by GAUSS for all-solid-state Li–S batteries

Single-atom catalysts with the maximum use of atom efficiency and metal–support interaction have been used for catalytic-related applications[5,10,28]. So far, studies of single-atom catalysts for Li–S batteries have been focused on liquid electrolytes[5,13]. Using single-atom catalysts to enhance all-solid-state Li–S batteries (ASSLSBs) is challenging owing to their limited catalytic activity in the solid-state systems. The unique structure of the Co/HGDY aerogel prepared by GAUSS provides abundant active sites for enhancing the sluggish Li–S redox reaction kinetics in all-solid-state Li–S batteries. A schematic of the Co/HGDY-enhanced ASSLSBs is shown in Fig. 4a. Here we synthesize active materials for sulfur cathodes by infiltrating sulfur into the Co/HGDY network (S@Co/HGDY) with a 9:1 mass ratio of sulfur to Co/HGDY.

As a control active material, we infiltrate sulfur into carbon black with a 9:1 sulfur to carbon mass ratio. Sulfur cathodes are made by mixing active material, carbon black and polyethylene oxide (PEO)/lithium bis(trifluoromethanesulfonyl)imide (LiTFSI) binder with a mass ratio of 0.6:0.15:0.25. Polyimide (PI) infiltrated with PEO@LiTFSI is used as the solid polymer electrolyte. Incorporating Co single atoms into the HGDY support enabled a maximum discharge capacity of ~900 mA h g^{-1} for ASSLSBs. A minimized overpotential of 0.15 V is obtained owing to the catalytic enhancement of Li–S conversion kinetics by Co single atoms (Fig. 4b). Larger polarizations are observed for the bare sulfur cathode (0.34 V) and S@HGDY cathode (0.28 V). Cyclic voltammetry measurements are performed to investigate the Li–S conversion for ASSLSBs using bare sulfur cathodes, and S@Co/HGDY cathodes at 60 °C. The S@Co/HGDY cathode shows a noticeable positive shift in the cathodic peak and a negative shift in the anodic peak (Supplementary Fig. 14), indicating the improved reaction kinetics of the S@Co/HGDY cathode owing to the function of the Co single atoms on HGDY.

Rate and cycling performance of sulfur cathodes with and without the Co/HGDY catalyst for ASSLSBs at 60 °C are shown in Fig. 4c. The catalytic effect of Co single atoms enhances the cycling and rate performance of the sulfur cathodes, in addition to decreasing the amount of soluble sulfur species in the solid polymer electrolytes by porous HGDY. The capacity and cycling stability of single-atom-enhanced ASSLSBs is comparable to state-of-the-art solid polymer-based ASSLSBs[29,30]. The specific surface area determined by Brunauer–Emmett–Teller is 1,000.5 $m^2 g^{-1}$ and 1,053.2 $m^2 g^{-1}$ for pure HGDY after sparking and Co/HGDY, respectively (Supplementary Fig. 15). Barrett–Joyner–Halenda pore size analysis shows that HGDY and Co/HGDY with a majority of pores less than 12 nm are favourable to accommodate the sulfur species (Supplementary Fig. 16).

The catalytic enhancement of the Li–S conversion reaction is supported by DFT calculations, which show a lower free energy for all steps in the conversion reaction (Fig. 4d). The optimized position for Co on HGDY, and optimized structures of the lithium polysulfide intermediates on the Co/HGDY substrate, are shown in the insets in Fig. 4d. The conversion from Li_2S_4 to Li_2S_2 and from Li_2S_2 to Li_2S have larger positive Gibbs free energy than the rest of the reaction steps, indicating that the formation of Li_2S_2 and Li_2S are rate-limiting steps in the discharge process. When considering Co single-atom catalysts in this conversion reaction, the energy barrier of Li_2S_4 to Li_2S_2 and Li_2S_2 to Li_2S is notably reduced. Experimental evidence of this catalytic effect is shown in the Li–S battery with S@Co/HGDY cathodes; a smaller ratio of the first plateau to second plateau (compared to the control cathode) in the voltage profile in Fig. 4b indicates that addition of Co/HGDY enables more Li_2S_4 conversion to Li_2S.

Conclusions

In summary, we developed a metastable nanomaterial synthesis platform, GAUSS, which can reach a high temperature of 3,286 K within only 8 ms. The high temperature and fast heating rate (~10^5 K s^{-1}) enables high-entropy and single-atom phases, while preventing phase separation, coarsening and ripening. As a result, a group of metastable nanomaterials (single atoms, high-entropy alloy nanoparticles and high-entropy oxide nanoparticles) were successfully synthesized using our GAUSS platform. The simplicity of our platform, combined with the ability to control the reaction time, temperature, composition and atmosphere, presents an efficient strategy to synthesize a wide range of metastable nanomaterials.

Online content

Any methods, additional references, Nature Portfolio reporting summaries, source data, extended data, supplementary information, acknowledgements, peer review information; details of author contributions and competing interests; and statements of data and code availability are available at https://doi.org/10.1038/s41565-022-01272-4.

References

1. Sun, W., Dacek, S., Ping Ong, S., Persson, K. & Ceder, G. The thermodynamic scale of inorganic crystalline metastability. *Sci. Adv.* **2**, e1600225 (2016).
2. Stein, A., Keller, S. W. & Mallouk, T. E. Turning down the heat: design and mechanism in solid-state synthesis. *Science* **259**, 1558–1564 (1993).
3. Yao, Y. et al. Carbothermal shock synthesis of high-entropy-alloy nanoparticles. *Science* **359**, 1489–1494 (2018).
4. Yao, Y. et al. High-throughput, combinatorial synthesis of multimetallic nanoclusters. *Proc. Natl Acad. Sci. USA* **117**, 6316–6322 (2020).
5. Zhou, G. et al. Theoretical calculation guided design of single-atom catalysts toward fast kinetic and long-life Li-S batteries. *Nano Lett.* **20**, 1252–1261 (2020).
6. Tian, H. et al. High-power lithium-selenium batteries enabled by atomic cobalt electrocatalyst in hollow carbon cathode. *Nat. Commun.* **11**, 5025 (2020).
7. Lun, Z. et al. Cation-disordered rocksalt-type high-entropy cathodes for Li-ion batteries. *Nat. Mater.* **20**, 214–221 (2021).
8. Pan, Q. et al. Gradient-cell–structured high-entropy alloy with exceptional strength and ductility. *Science* **374**, 984–989 (2021).
9. Li, Z., Pradeep, K. G., Deng, Y., Raabe, D. & Tasan, C. C. Metastable high-entropy dual-phase alloys overcome the strength-ductility trade-off. *Nature* **534**, 227–230 (2016).
10. Wei, H. et al. Iced photochemical reduction to synthesize atomically dispersed metals by suppressing nanocrystal growth. *Nat. Commun.* **8**, 1490 (2017).
11. Xia, C. et al. General synthesis of single-atom catalysts with high metal loading using graphene quantum dots. *Nat. Chem.* **13**, 887–894 (2021).
12. Xie, P. et al. Highly efficient decomposition of ammonia using high-entropy alloy catalysts. *Nat. Commun.* **10**, 4011 (2019).
13. Du, Z. et al. Cobalt in nitrogen-doped graphene as single-atom catalyst for high-sulfur content lithium-sulfur batteries. *J. Am. Chem. Soc.* **141**, 3977–3985 (2019).
14. Jiang, K. et al. Isolated Ni single atoms in graphene nanosheets for high-performance CO_2 reduction. *Energy Environ. Sci.* **11**, 893–903 (2018).
15. Kitchen, H. J. et al. Modern microwave methods in solid-state inorganic materials chemistry: from fundamentals to manufacturing. *Chem. Rev.* **114**, 1170–1206 (2014).
16. Chen, C. H. et al. Ruthenium-based single-atom alloy with high electrocatalytic activity for hydrogen evolution. *Adv. Energy Mater.* **9**, 1803913 (2019).
17. Feng, J. et al. Unconventional alloys confined in nanoparticles: building blocks for new matter. *Matter* **3**, 1646–1663 (2020).
18. Wang, X. et al. Continuous 2,000 K droplet-to-particle synthesis. *Mater. Today* **35**, 106–114 (2020).
19. Yang, Y. et al. Aerosol synthesis of high entropy alloy nanoparticles. *Langmuir* **36**, 1985–1992 (2020).
20. Qiao, H. et al. Scalable synthesis of high entropy alloy nanoparticles by microwave heating. *ACS Nano* **15**, 14928–14937 (2021).
21. Xie, H. et al. A high-temperature pulse method for nanoparticle redispersion. *J. Am. Chem. Soc.* **142**, 17364–17371 (2020).
22. Li, H. et al. Nano high-entropy materials: synthesis strategies and catalytic applications. *Small Struct.* **1**, 2000033 (2020).
23. Wang, C. et al. A general method to synthesize and sinter bulk ceramics in seconds. *Science* **368**, 521–526 (2020).
24. Gao, X., Liu, H., Wang, D. & Zhang, J. Graphdiyne: synthesis, properties, and applications. *Chem. Soc. Rev.* **48**, 908–936 (2019).
25. Du, R. et al. CMP aerogels: ultrahigh-surface-area carbon-based monolithic materials with superb sorption performance. *Adv. Mater.* **26**, 8053–8058 (2014).

26. Xue, Y. et al. Anchoring zero valence single atoms of nickel and iron on graphdiyne for hydrogen evolution. *Nat. Commun.* **9**, 1460 (2018).
27. Yao, Y. et al. High temperature shockwave stabilized single atoms. *Nat. Nanotechnol.* **14**, 851–857 (2019).
28. Yao, S. & Zhang, X. Atomic-layered Au clusters on α-MoC as catalysts for the low-temperature water-gas shift reaction. *Science* **357**, 389–393 (2017).
29. Zhang, H. et al. Designer anion enabling solid-state lithium-sulfur batteries. *Joule* **3**, 1689–1702 (2019).
30. Gao, X. et al. All-solid-state lithium-sulfur batteries enhanced by redox mediators. *J. Am. Chem. Soc.* **143**, 18188–18195 (2021).
31. Yao, Y. et al. Computationally aided, entropy-driven synthesis of highly efficient and durable multi-elemental alloy catalysts. *Sci. Adv.* **6**, eaaz0510 (2020).
32. Yang, H. et al. Carbon dioxide electroreduction on single-atom nickel decorated carbon membranes with industry compatible current densities. *Nat. Commun.* **11**, 593 (2020).
33. Zhu, Y. et al. A cocoon silk chemistry strategy to ultrathin N-doped carbon nanosheet with metal single-site catalysts. *Nat. Commun.* **9**, 3861 (2018).
34. Yang, H. et al. A universal ligand mediated method for large scale synthesis of transition metal single atom catalysts. *Nat. Commun.* **10**, 4585 (2019).

Methods

Synthesis of metastable nanomaterials using GAUSS platform

HGDY aerogel was synthesized by a Glaser coupling reaction[25]. The HGDY aerogel was obtained by dissolving 30 mg 1,3,5-triethynylbenzene and 6 mg CuCl in pyridine (2 ml), conducting the reaction in the water bath at 40 °C for 72 h to form HGDY gel, washing with pyridine, chloroform, methanol, ethanol and deionized water, and, finally, freeze drying. For Co single-atom synthesis, $CoCl_2$ was dissolved in ethanol with a dilute concentration of 0.1 mM as Co precursors. Solvated HGDY was obtained by dropping Co precursors onto the HGDY aerogel. The HGDY aerogel with metal chloride precursors was obtained by drying the solvated HGDY for 24 h. To perform the GAUSS reaction, the HGDY aerogel was put into contact with the hotplate at 450 °C in the glovebox. When the HGDY aerogel touched the hotplate (set to 450 °C), ignition occurred at a single point. During the reaction, red flames spread quickly from the origin through the entire aerogel, transforming the HGDY from a light brown to a black colour. This reaction produces a significant amount of heat and pressure. Co nanoparticles were obtained by using 5 mM $CoCl_2{\cdot}6H_2O$ precursor. For synthesis of NiFeCoCuSnMo high-entropy alloys, corresponding metal chlorides with a concentration of 0.05 mol l^{-1} were dissolved in ethanol. The metal chloride precursors were well mixed equally and added onto HGDY to form solvated HGDY. NiFeCoCuSnMo high-entropy oxides were synthesized following a process similar to that for the NiFeCoCuSnMo high-entropy alloys except performing the GAUSS reaction in oxygen-rich atmosphere. Physical properties of the metal chloride precursors and metals used in the preparation are shown in Supplementary Table 4. To tune the temperature and ramping speed of heating, aluminium nanoparticles and sodium perchlorate ($NaClO_4$) oxidizers were dissolved in ethanol and adsorbed onto HGDY. The highest temperature of 3,286 K at 8 ms was obtained with a mass ratio of HGDY:Al:$NaClO_4$ of 3:3:5.

Electrochemical measurement

Commercial sulfur was infiltrated into the Co/HGDY framework and served as the active material in the cathode. Commercial sulfur with carbon black was used as a control. The mass ratio of sulfur to Co/HGDY was 9:1. To form the sulfur cathode, 60% active material, 15% carbon black and 25% PEO/LiTFSI were used. The mass ratio of PEO (M_w, 300 K):LiTFSI was 3:2. Polyimide infiltrated with PEO@LiTFSI was used as the solid polymer electrolyte[35]. The mass loading of sulfur in the cathode was 0.4–0.5 mg cm^{-2}. In an argon-filled glovebox, 2032-type coin cells were assembled using sulfur cathodes, polyimide with PEO@LiTFSI electrolytes and lithium metal anodes. Coin cells were loaded into a battery tester (Land Instruments) and cycled between 1.6 V and 2.8 V. The temperature was controlled by an environmental chamber (BTU-133, ESPEC North America). The cyclic voltammetry were performed on a Bio-Logic VMP3 electrochemical workstation.

Characterizations

Transmission electron microscopy images and elemental mapping of high-entropy oxides were recorded on a Titan instrument. High-speed videos were taken using a high-speed camera (Photron FASTCAM SA5) at 5,000 fps. Temperature evolution from the GAUSS was measured using a high-speed infrared camera (FLIR X6900sc MWIR) at 1,000 fps. XPS was carried out using a PHI instrument. Co K-edge X-ray absorption spectroscopy were recorded at Beamline 4–1 of the Stanford Synchrotron Radiation Light Source. The gas products evolved from GAUSS were measured using gas chromatography (GC SRI Instruments 8610C). Nitrogen isothermal adsorption/desorption measurements were performed using an Autosorb iQ Station. Inductively Coupled Plasma Optical Emission Spectrometer (ICP-OES) were performed on a Thermo Scientific ICAP 6300 Duo View Spectrometer. The amount of oxygen was undefined.

COMSOL simulation. COMSOL Multiphysics v.5.5 was used to simulate the temperature evolution of HGDY induced by GAUSS. The transient analysis was performed using the 'heat transfer in porous media' module integrated in COMSOL. We first investigated the heating behaviour of HGDY. The porous sample was composed of the HGDY matrix with empty space filled by air. Physical properties of the materials used in the numerical modelling are shown in Supplementary Table 5. We used the heating source from the GAUSS reaction and the heat loss to the environment to reveal the temperature evolution of the HGDY. The sparking heating was supplied by a constant volumetric heat source (2.15×10^9 W m^{-3}) in the sample for 20 ms. The heat flux from the sample surface to the surrounding environment (for example, heat loss) was given by the following equation: $q = h(T_{ext} - T)$, where q is the heat flux, T_{ext} the external temperature (293 K), T the temperature of the cell surface and h the heat transfer coefficient (5 W m^{-2} K^{-1}).

DFT calculations. The calculations of reduction of sulfur and lithium polysulfide (Li_2S_x) molecules on HGDY substrate were performed using the DFT code GPAW[36,37]. Plane-wave cutoff of 600 eV and Γ point Brillouin zone sampling were adopted for all calculations to ensure proper self-consistent field convergence. The slabs were created with an empty space of 20 Å in the z direction to describe the vacuum environment. The energy and force convergence criteria were set to be 10^{-4} eV per cell and 10^{-3} eV $Å^{-1}$, respectively. The non-local exchange-correlation functional vdw_df_cx was used to model dispersion interaction between the adsorbate and the substrate[38]. The relative energies for the following reduction reactions were determined:

$$S_8 + 2Li^+ + 2e^- \rightarrow Li_2S_8,$$

$$Li_2S_8 + (2/3)\,Li^+ + (2/3)\,e^- \rightarrow (4/3)\,Li_2S_6,$$

$$Li_2S_6 + Li^+ + e^- \rightarrow (3/2)\,Li_2S_4,$$

$$Li_2S_4 + 2Li^+ + 2e^- \rightarrow 2Li_2S_2,$$

$$Li_2S_2 + 2Li^+ + 2e^- \rightarrow 2Li_2S.$$

The energy of each substance involved in the reactions was calculated as the total energy of the reactant/product plus the HGDY substrate (and single-atom Co if present). The structural minimization was performed for each case to obtain the lowest energy geometry of the adsorbate.

Data availability

The data that support this study are included in the article and/or supplementary information. Any additional materials and data are available from the corresponding authors on reasonable request.

References

35. Wan, J. et al. Ultrathin, flexible, solid polymer composite electrolyte enabled with aligned nanoporous host for lithium batteries. *Nat. Nanotechnol.* **14**, 705–711 (2019).
36. Mortensen, J. J., Hansen, H. A. & Jacobsen, K. Real-space grid implementation of the projector augmented wave method. *Phys. Rev. B* **71**, 035109 (2005).
37. Enkovaara, J. et al. Electronic structure calculations with GPAW: a real-space implementation of the projector augmented-wave method. *J. Phys. Condens Matter* **22**, 253202 (2010).
38. Berland, K. & Hyldgaard, P. Exchange functional that tests the robustness of the plasmon description of the van der Waals density functional. *Phys. Rev. B* **89**, 035412 (2014).

Acknowledgements

This work was jointly supported by the US Department of Energy (DOE), Office of Basic Energy Sciences, Division of Materials Sciences and Engineering (contract no. DE-AC02-76SF00515) and the Assistant

Secretary for Energy Efficiency and Renewable Energy, Office of Vehicle Technologies, of the US Department of Energy under the Battery Materials Research (BMR) Program and the Battery500 Consortium program. We acknowledge H. Gong for freeze drying of the HGDY aerogel. Use of the Stanford Synchrotron Radiation Light Source, SLAC National Accelerator Laboratory, is supported by the US DOE, Office of Science, Office of Basic Energy Sciences under contract DE-AC02-76SF00515. Part of this work was performed at the Stanford Nano Shared Facilities (SNSF), supported by the National Science Foundation under award ECCS-2026822. Characterization done by the UCI team (R.Z. and H.L.X.) was supported by the National Science Foundation under award number CHE-1900401 and H.L.X.'s startup funding. We acknowledge the use of facilities and instrumentation at the UC Irvine Materials Research Institute (IMRI), which is supported in part by the National Science Foundation through the UC Irvine Center for Complex and Active Materials (DMR-2011967). Part of the work was supported by the Office of Naval Research under agreement number N00014-22-1-2489.

Author contributions

Y.C., Xueli Zheng and X.G. conceived the idea. Y.C. supervised the project. Xueli Zheng and X.G. designed and carried out all the experiments. Xueli Zheng, X.G., Y.J. and Xiaolin Zheng helped with high-speed video and thermal video measurements. R.A.V., R.Z. and H.L.X. performed S/TEM measurements. X.X. performed gas chromatography experiments. R.X. performed COMSOL simulations. J.W. carried out DFT calculations. Y.Y. performed XPS measurements. P.Z., Y.Y. and L.C.G. assisted with materials synthesis. All authors discussed the results and assisted during manuscript preparation.

Competing interests

The authors declare no competing interests.

Additional information

Supplementary information The online version contains supplementary material available at https://doi.org/10.1038/s41565-022-01272-4.

Correspondence and requests for materials should be addressed to Yi Cui.